Ultrafast operation of a mode-locked Ti:sapphire laser

Edwin Ng[*,1] **and Tatsuhiro Onodera**[1]

Department of [1]*Applied Physics, Stanford University*
[*]*Report author: edwin98@stanford.edu*

Compiled March 22, 2015

The properties of a Ti:sapphire laser pumped at 532 nm are explored. We characterize the Ti:sapphire gain bandwidth and laser output in CW mode, and then adjust the cavity dispersion to achieve pulsed, mode-locked operation at 92.5 MHz. Measurements of bandwidth, peak wavelength, and pulse width are performed with an optical spectrum analyzer and a Michelson interferometric intensity autocorrelator. We measure pulse widths between 30 fs and 40 fs, bandwidths between 30 nm and 70 nm, and peak wavelength tuning between 835 nm and 865 nm. Time-bandwidth products are computed and compared to the Fourier transform limit. Dispersive elements (ZnSe and silica) are introduced to observe pulse broadening. © 2015 Optical Society of America

OCIS codes: (140.4050) Mode-locked lasers; (140.3590) Lasers, titanium; (140.7090) Ultrafast lasers

1. Introduction

The key to doing nonlinear optics is to use light sources with high peak powers. The large electric fields created by such sources facilitates efficient generation of a rich variety of phenomena tied to strong interactions between light and matter: higher harmonic generation, parametric amplification, multi-photon absorption, and so on. Among the best candidates to fill this role are mode-locked lasers, which have a wide gain bandwidth supporting a large number (upwards of 10^5) modes that—when locked together in phase—produce extremely short (sub-ps) pulses with very high peak power (compared to say Q-switching). The importance of these mode-locked lasers extends even beyond nonlinear optics: the wide, evenly spaced "frequency comb" embedded in the ultrafast output serves as an exquisite frequency reference for precision metrology and spectroscopy. [1]

Perhaps the most dominant mode-locked laser gain medium is the titanium-doped sapphire (Ti:Al$_2$O$_3$ or Ti:sapphire) crystal, CW-pumped at 532 nm. The Ti:sapphire has a broad emission spectrum from about 650 nm to 1100 nm, capable of supporting a large number of resonator modes separated by the cavity FSR. In CW mode, only one of these modes ends up lasing, and the result is a highly tunable CW laser.

To achieve mode-locked operation, one common method is to take advantage of the nonlinear Kerr effect, in which high intensity pulses induce a lens in the Ti:sapphire crystal itself. If the cavity is slightly destabilized away from optimal CW operation, (e.g., by adding a slit to restrict the mode size), high-intensity pulses are favored since the Kerr lens refocuses the intracavity mode to reduce losses. A perturbation can then induce a mode-locked state from noise, which is then sustained provided the dispersion in the cavity caused by the mirrors and crystal are correctly compensated. [1]

This AP304 lab traditionally uses a Tsunami Ti:sapphire laser, but in this report, we opt instead to discuss recent measurements made in the Mabuchi Lab to characterize a KM Labs Model MTS Mini Ti:sapphire

laser to be used for future experiments in nonlinear and ultrafast optics. The measurements were performed by E.N. and T.O. in the week of March 16, 2015 and are modeled directly after the procedures described in [2]. We hope thereby to emphasize the applicability of AP304 material to a research (albeit diagnostic) setting.

The layout of the laser is shown in Fig. 1. The laser is pumped by a Coherent Verdi G5 at 532 nm, which is set around 4.6 W to 4.7 W for most of the CW measurements and all the mode-locked measurements. The laser has only recently been realigned after a long hiatus, and—as our measurements show—several more iterations are needed before it is suitable as a robust light source.

The main degrees of freedom we adjust in this lab are: the location of the second curved mirror (6 in Fig. 1), the translation of the second prism (8 in Fig. 1) in and out of the beam path, and the alignment of the HR and OC (9 and 1 respectively in Fig. 1). By moving the second pump mirror towards the crystal, the waist becomes small at the focus in the crystal, thus destabilizing the cavity mode in CW operation and promoting the onset of mode-locked operation.

2. CW operation

CW operation is the initial state of the laser without perturbation or when the dispersion compensation of the two prisms is set away from the mode-locked range. In CW mode, we find that translating the prism gives an effective wavelength tuning despite the absence of a wavelength-selective slit. This is likely because the dispersed beam from the first prism clips to some extent at the second prism, giving rise to a wavelength preference as the latter is translated.

We are interested in measuring the CW output power as a function of the wavelength, which should give us an idea of the gain bandwidth of the Ti:sapphire crystal. To make this measurement, we use a (silver) flipper mirror to switch the output between going to a compact CCD grating spectrometer and an optical power meter with a green bandstop filter (OD 6+) in front to remove the small reflected pump light in the output.
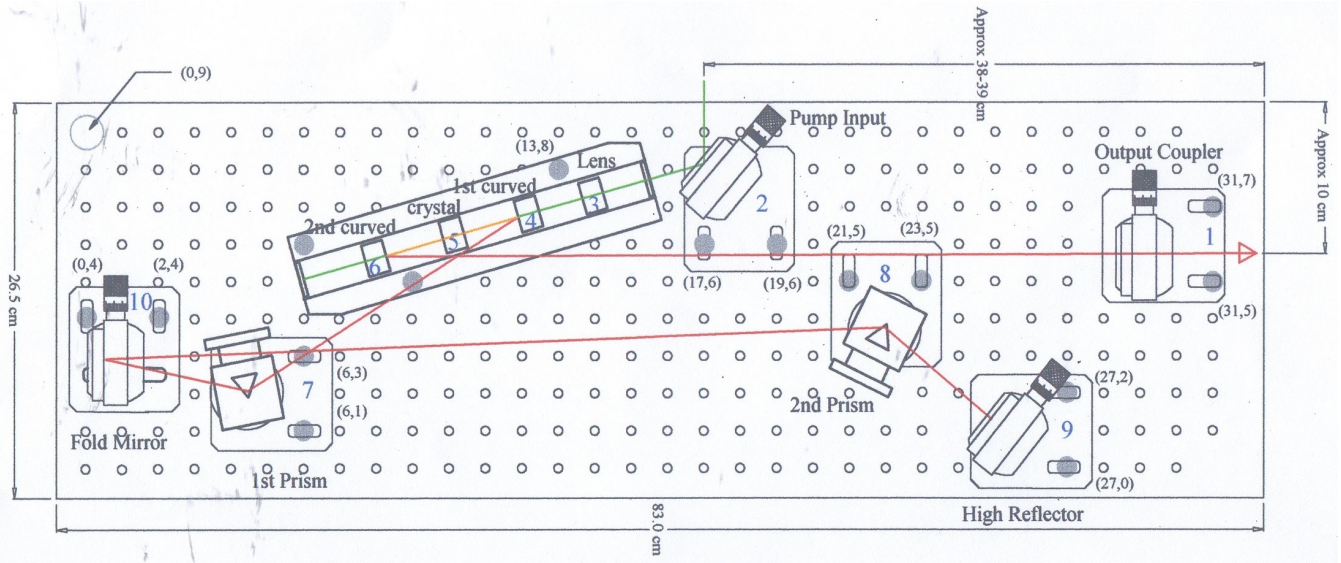
Fig. 1. Layout of the laser as recommended by KM Labs, adapted from their manual. [3]. The notated values are for guidance only and do not reflect actual values used in the present alignment. The red line indicates the cavity mode and the green line, the pump beam.

Fig. 2 shows the output power as a function of the accessible wavelengths, with the pump mirror set far, to promote CW lasing. It is interesting to note that we are unable to tune the entire range of the Ti:sapphire gain bandwidth, as the wavelength tuning stops around 810 nm; the laser continues to lase but the wavelength is clamped with further translation of the prism. However, the partial results obtained are consistent with a previous measurement of the full gain bandwidth of the Ti:sapphire using the Tsunami laser (inset in Fig. 2). This restriction is potentially problematic, as it could limit the bandwidth available for mode-locking and is thus worth investigating futher; perhaps moving the first prism could change the available range.

Another relevant measurement is the output power of the laser as a function of pump, which we show in Fig. 3 for two different pump mirror configurations. In the case where the pump mirror is far, we obtain a relatively low threshold of 2.7 W pump, with a slope efficiency of 20 %. There is a noticeable change in the system occurring around 4.2 W of pump, where the slope droops slightly.

We also notice that by moving the pump mirror forward, the lasing threshold and slope efficiency of the CW mode are detrimentally affected. Because the cavity mode is now focused more tightly at the crystal, it is diverging more rapidly elsewhere, leading to higher losses. Operating of the laser in this state with the right dispersion compensation is the key to mode-locking.
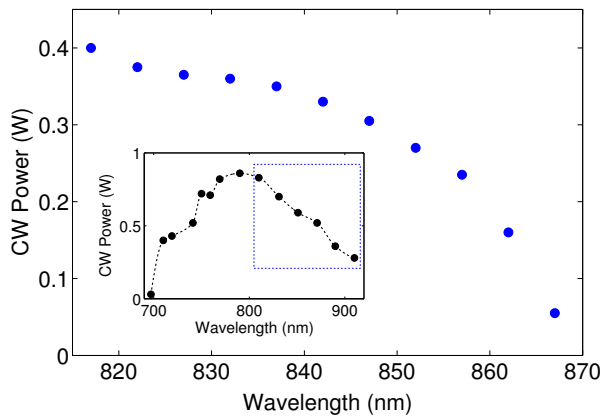

Fig. 2. CW output as a function of accessible wavelengths, as the second prism is translated. Inset: A full gain profile measured on the Tsunami Ti:sapphire system. Box indicates the approximate regime of accessible wavelengths in present setup.
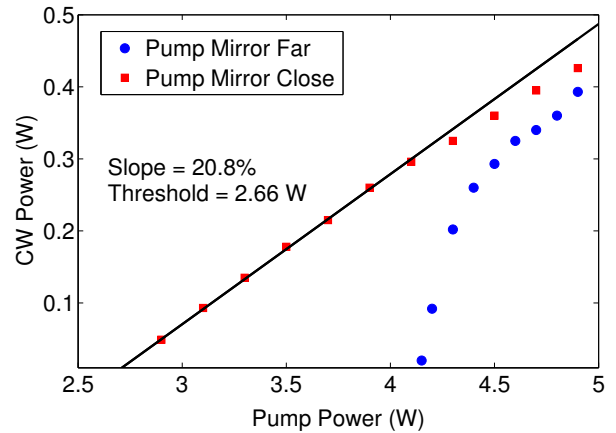

Fig. 3. CW output as a function of pump power, for two different configurations of the pump mirror. The translation of the mirror between the two cases is approximately 3 mm. The solid line indicates a fit to the linear portion of the data.

2

3. Mode-locked operation

When the pump mirror and the second prism are in approximately the right range, a perturbation such as a sudden motion of the prism can cause the cavity to mode-lock. A fast photodiode monitoring the output via a pickoff gives the first indication of pulsing, as shown by the trace inset in Fig. 4. Although the photodiode is nowhere near fast enough to resolve the pulses in time, it does give us a good estimate of the repetition rate, which is found from the trace to be approximately 92.5 MHz. Since the repetition rate depends mostly on the cavity length, we do not expect this value to change much.

In order to obtain information about the pulse shape in time, we must resort to indirect means. Among the most accessible methods is to use an interferometric intensity autocorrelator (IIAC), which overlaps the pulse train with a version of itself, but shifted by some known delay. By doing an interference measurement between the two pulse trains as a function of delay, information about the pulse intensity (but not phase) is obtained.

For this experiment, we use a Michelson-based IIAC as described in [4]. The passive arm of the Michelson is mounted on a micrometer for calibration of the path length difference, while the active arm is mounted onto a speaker driven with a function generator to scan the path length and hence delay of this arm. Gold retroreflectors are used to minimize beam deflection during the active arm travel. A GaP detector is used to detect the interference between the two pulse trains. The signal at the GaP detector (bandgap 550 nm) is mostly composed of two-photon absorption events, thus implementing a nonlinear measurement of the pulse overlap. [4]
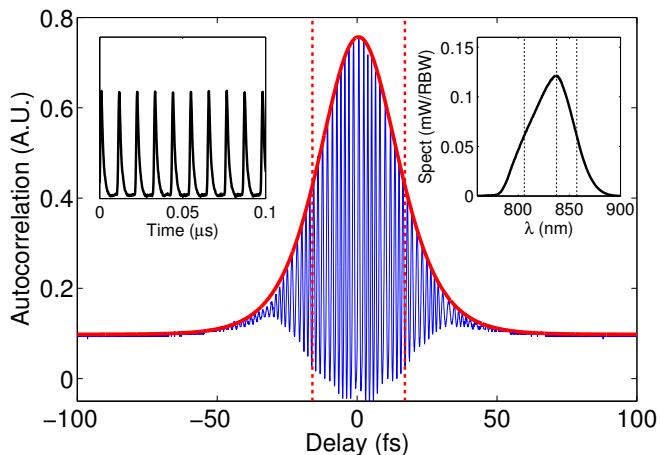

Fig. 4. Typical trace obtained when doing an IIAC measurement on the mode-locked output. The red curve denotes the fitted envelope, with the half-maximum points denoted by red dotted lines. The delay is found from the time trace using method described in main text. Insets: Left, PD trace of the pulsed output; Right, OSA trace showing the corresponding spectrum, with center and half-maximum points indicated with dashed lines.

In more detail, if the output of the laser is described by the electric field $E(t)$, then the IIAC measures $I_{AC}(\tau) = \int |E(t) + E(t+\tau)|^4 \, dt$. We can describe some qualitative features of such a signal. First, there are typical interference fringes due to the beating between the electric field oscillations of the two pulses. Second, there is always a background signal due to the average output power, which is related to the peak by a factor of $1/8$. Finally, and most importantly, the envelope of these fringes is directly related to the pulse shape, and measurement of the FWHM of this envelope then translates to the FWHM of the pulse intensity $E^2(t)$ via a geometric factor based on the pulse shape. [4]

But to utilize the IIAC we need to also calibrate the delay time. We do this by noting that there is only a signal when the two arms are balanced in length to allow overlap of the pulses in some given repetition period, to within the speaker drive. Thus, we turn the micrometer on the passive arm until we lose signal at the peaks and troughs of the speaker scan, and use the difference to deduce the scan amplitude, which we found to be $A_0 = 0.0575$ mm at a sinusoidal drive voltage of 7.7 V_{pp}. The speaker frequency is set to $f_0 = 4.9$ Hz, which gives enough time to see the fringes on the photodetector.

We deduce that $\tau = A_0 \sin(2\pi f_0 t)$, where t is the measured time on the scope. In this way, we convert the abscissa on all our IIAC traces to τ. We translate the passive arm until the peak of the IIAC signal occurs at the nominal zero of the drive, so that the drive is most linear near the signal.

Finally, to convert the IIAC traces to the actual FWHM pulse width, we extract the peaks of the interference pattern and fit a $sech^2$ function (with background) to the envelope. We extract the FWHM numerically, and then divide by 1.54 to obtain the actual pulse width, assuming the pulse shape is given by $sech^2$. [1] The choice to use a $sech^2$ as the fit function is arbitrary and also conceptually separate from the assumption that the pulse shape is $sech^2$. Nevertheless, we find that the $sech^2$ pulse shape gives the most sensible results in terms of the time-bandwidth product, as discussed below and in more depth by T.O.

Fig. 5 summarizes the pulse widths, bandwidths, and time-bandwidth products for this experiment, with the various data points obtained as we translate the second prism to vary the dispersion compensation. Interestingly, the "sweet spot" where the bandwidth starts to increase rapidly also features little wavelength tuning (hence the vertical asymptotes). The two data sets are taken with the same cavity configuration, except the pump laser was turned down about 2 W and then turned back up. Significant nonlinearity/hysteresis is thus evident.

Furthermore, we see from the time-bandwidth product that although the bandwidth increases, the measured pulse width does not decrease enough to keep the product constant. This indicates dispersion in the beam which broadens the pulse. Further work is necessary to find an operating point close to the Fourier limit.
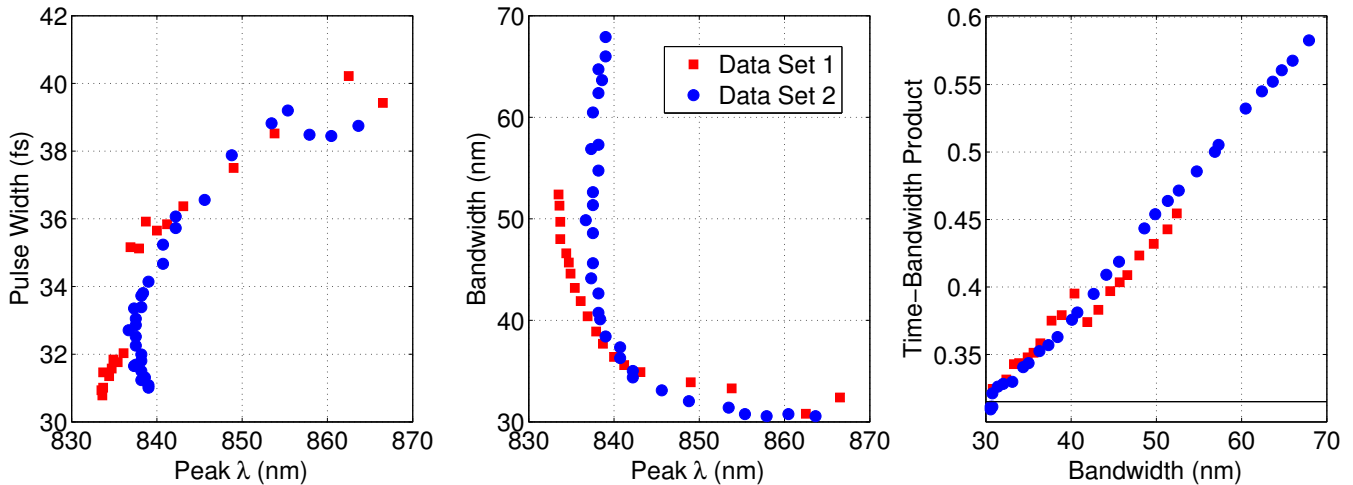
Fig. 5. Pulse width, bandwidth, and time-bandwidth product data. The pulse widths are obtained as described in main text. Bandwidth $\Delta\lambda$ is recorded by taking an OSA trace and looking $-3\,\mathrm{dB}$ down from peak. The time bandwidth product is the product of the pulse width and $c\Delta\lambda/\lambda^2$, divided by 1.54 for the pulse shape. The solid line in the right plot shows the Fourier limited product of 0.315 for these pulses.

Finally, we can also try introducing various materials into the beam path in order to observe pulse broadening due to dispersion. We set the prism position such that we get pulses with a bandwidth of approximately 60 nm, at center wavelength 827 nm. Since dispersive materials usually introduce a frequency chirp (where there is a changing frequency profile in the pulse), the IIAC fringes disappear in a broad, elongated wing around the central fringes. It is the envelope of this whole profile gives the actual pulse width.

We note because of these highly dispersed pulses, a better way of defining the FWHM is to actually low pass the signal and read off the filtered envelope. This definition is the one suggested in [4], and generally yields different results from the more naive approach described above, especially for chirped pulses.
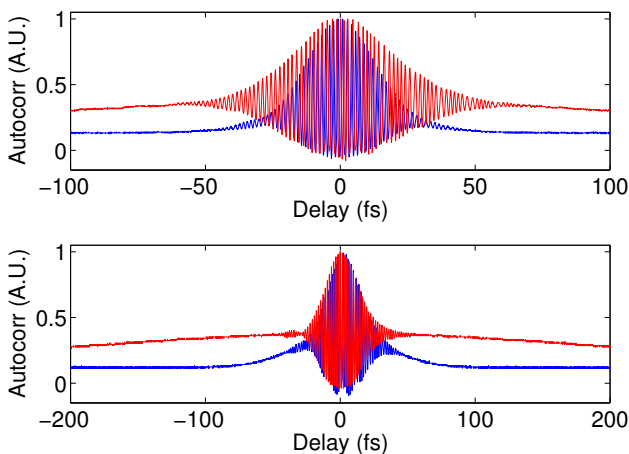

Fig. 6. Pulse broadening due to dispersive optics. Red trace shows IIAC trace with the dispersive optic in place and blue without. Note that the traces have been normalized for direct comparison.

The first case is a ZnSe plate of thickness 3 mm, shown at top in Fig. 6. We see significant broadening of the pulse in the wings, which do not reach their constant background level even within this entire trace. We calculate the FWHM pulse width to be about 220 fs, compared to the initial pulse with about 40 fs.

Alternatively, we also try a piece of 10 cm fused silica, shown at bottom in Fig. 6. Again, we see broadening of the pulse and the development of wings. We calculate the FWHM pulse width to be about 270 fs, compared to the initial pulse width of about 70 fs.

4. Conclusions

We characterize a work-in-progress Ti:sapphire laser in both CW and mode-locked operation regimes. In CW mode, we measure the output power as a function of wavelength tuning and pump power. The laser output is found to be highly dependent on the position of the second prism and pump mirror.

We use a Michelson-based IIAC to measure the pulse widths of the laser output in mode-locked operation. By comparing the measured pulse widths to the measured optical bandwidth, we find that the pulses are generally not quite Fourier-transform limited. Additional progress on this front is expected.

References

1. J.-C. Diels and W. Rudolph, *Ultrashort Laser Pulse Phenomena*, (Academic Press, 1996).
2. AP304 Staff, "Experiment 7: Modelocked Ti:Sapphire Laser" (unpublished lab manual).
3. Kapteyn-Murnane Laboratories, L.L.C., Model MTS Ti:Sapphire Laser Kit Instruction Manual (unpublished, not for general distribution).
4. AP305 Staff, "Experiment 5: Nonlinear Fiber Continuum Generation" (unpublished lab manual).